Daydreamer, a Ras effector and GSK-3 substrate, is important for directional sensing and cell motility

Koelsch, Verena; Shen, Zhouxin; Lee, Susan; Plak, Katarzyna; Lotfi, Pouya; Chang, Jessica; Charest, Pascale G.; Romero, Jesus Lacal; Jeon, Taeck J.; Kortholt, Arjan

Published in:
Molecular Biology of the Cell

DOI:
10.1091/mbc.E12-04-0271

Publication date:
2013

Daydreamer, a Ras effector and GSK-3 substrate, is important for directional sensing and cell motility

Verena Kölsch[a,*], Zhouxin Shen[a], Susan Lee[a], Katarzyna Plak[b], Pouya Lotfi[a], Jessica Chang[a], Pascale G. Charest[a,c], Jesus Lacal Romero[a], Taeck J. Jeon[a,†], Arjan Kortholt[b], Steven P. Briggs[a], and Richard A. Firtel[a,c]

[a]Section of Cell and Developmental Biology, Division of Biological Sciences, University of California, San Diego, La Jolla, CA 92093-0380; [b]Department of Molecular Cell Biology, University of Groningen, 9751 NN Haven, The Netherlands; [c]University of Arizona, Department of Chemistry and Biochemistry, Tucson, AZ 85721-0088

ABSTRACT **How independent signaling pathways are integrated to holistically control a biological process is not well understood. We have identified Daydreamer (DydA), a new member of the Mig10/RIAM/lamellipodin (MRL) family of adaptor proteins that localizes to the leading edge of the cell. DydA is a putative Ras effector that is required for cell polarization and directional movement during chemotaxis. *dydA*$^-$ cells exhibit elevated F-actin and assembled myosin II (MyoII), increased and extended phosphoinositide-3-kinase (PI3K) activity, and extended phosphorylation of the activation loop of PKB and PKBR1, suggesting that DydA is involved in the negative regulation of these pathways. DydA is phosphorylated by glycogen synthase kinase-3 (GSK-3), which is required for some, but not all, of DydA's functions, including the proper regulation of PKB and PKBR1 and MyoII assembly. *gskA*$^-$ cells exhibit very strong chemotactic phenotypes, as previously described, but exhibit an increased rate of random motility. *gskA*$^-$ cells have a reduced MyoII response and a reduced level of phosphatidylinositol (3,4,5)-triphosphate production, but a highly extended recruitment of PI3K to the plasma membrane and highly extended kinetics of PKB and PKBR1 activation. Our results demonstrate that GSK-3 function is essential for chemotaxis, regulating multiple substrates, and that one of these effectors, DydA, plays a key function in the dynamic regulation of chemotaxis.**

Monitoring Editor
David G. Drubin
University of California, Berkeley

Received: Apr 10, 2012
Revised: Oct 22, 2012
Accepted: Nov 1, 2012

This article was published online ahead of print in MBoC in Press (http://www.molbiolcell.org/cgi/doi/10.1091/mbc.E12-04-0271) on November 7, 2012.

Present addresses: *Gerhard-Domagk-Institut für Pathologie, Universitätsklinikum Münster, 48149 Münster, Germany; †Department of Biology, College of Natural Sciences, Chosun University, Gwangju 501-759, Korea.

Address correspondence to: Richard A. Firtel (rafirtel@ucsd.edu).

Abbreviations used: AL, activation loop; CH, calponin homology; DydA, Daydreamer; *dydA*$^-$, DydA-null; GFP, green fluorescent protein; GSK-3, glycogen synthase kinase-3; *gskA*$^-$, GSK-3–null; GST, glutathione *S*-transferase; HHF, His-HA-FLAG; HM, hydrophobic motif; IMP-A, inositol monophosphatase; mGppNHP, 2′/3′-O-(N-Methylanthraniloyl)-guanosine-5′-[(β,γ)-imido]triphosphate; MRL, Mig10/RIAM/lamellipodin; MyoII, myosin II; pan, α–phospho-protein kinase C; PH, pleckstrin homology; PI(3)P, phosphatidylinositol 3-phosphate; PI(3,4)P_2, phosphatidylinositol (3,4)-bisphosphate; PI(3,4,5)P_3, phosphatidylinositol (3,4,5)-triphosphate; PI3K, phosphoinositide-3-kinase; PRM, proline-rich motif; RA, Ras association; RBD, Ras-binding domain; TORC2, target of rapamycin complex 2.

INTRODUCTION

Chemotaxis, or directed cell movement up a chemoattractant gradient, plays a key role in a range of biological processes, including innate immunity, metastasis of cancer cells, tissue development, food foraging, and the formation of multicellular structures in free-living organisms such as *Dictyostelium* (Eccles, 2004; Martin and Parkhurst, 2004; Böttcher and Niehrs, 2005; Sasaki and Firtel, 2006). Cells are able to sense extracellular gradients as shallow as a 2% difference in chemoattractant concentration across the cell and are able to amplify that gradient intracellularly to produce a highly polarized cell in which the activity of leading edge– and posterior-specific signaling components are highly restricted to the respective poles of the cell (Van Haastert and Veltman, 2007; Janetopoulos and Firtel, 2008; Kölsch *et al*., 2008). The Ras family of small GTPases, including Ras and Rap1, are key upstream regulators of directional sensing and chemotaxis. *Dictyostelium* cells in which Ras function has been abrogated exhibit delayed polarization when placed in a

chemoattractant gradient and, once polarized, move randomly, being unable to sense the direction of the gradient (Sasaki *et al*., 2004). Proper spatiotemporal regulation of at least two Ras-mediated pathways is required in *Dictyostelium* for efficient directed migration: the class 1 phosphoinositide-3-kinase (PI3K) pathway, which is activated predominantly by RasG, and the target of rapamycin complex 2 (TORC2) pathway, which is activated predominantly by RasC (Lee *et al*., 1999; Funamoto *et al*., 2002; Sasaki *et al*., 2004, 2007; Sasaki and Firtel, 2006; Bolourani *et al*., 2006; Charest *et al*., 2010). PI3K and TORC2 lead to the local activation of Akt/PKB and the related kinase PKBR1 and other downstream effectors, resulting in changes in the cytoskeleton and directed migration (Kamimura *et al*., 2008; Kamimura and Devreotes, 2010; Charest *et al*., 2010). Efficient chemotaxis has also been shown to require additional Ras and Rap1 effectors, signaling from guanylyl cyclase and phospholipase A2, and, more recently, glycogen synthase kinase-3 (GSK-3; Veltman and Van Haastert, 2006; Veltman *et al*., 2008; van Haastert *et al*., 2007; Chen *et al*., 2007; Teo *et al*., 2010; Kim *et al*., 2011).

GSK-3, identified in mammalian cells as a kinase that phosphorylates and regulates glycogen synthase, controls a wide range of biological processes, including insulin and Wnt signaling, cell survival, neuronal development, and cell migration (Embi *et al*., 1980; Hemmings *et al*., 1981; Cross *et al*., 1995; Pap and Cooper, 1998; Papkoff and Aikawa, 1998; Kozlovsky *et al*., 2002; Manoukian and Woodgett, 2002; reviewed in Jope and Johnson, 2004; Kim *et al*., 2009). *Dictyostelium* GSK-3 was discovered in a genetic screen for regulators of cell fate determination (Harwood *et al*., 1995; Kawata *et al*., 1997; Ginger *et al*., 2000; Grimson *et al*., 2000) and subsequently demonstrated to be required for chemotaxis (Teo *et al*., 2010; Kim *et al*., 2011). GSK-3–null (*gskA*$^-$) cells move more slowly and have a deeply decreased directionality when compared with wild-type cells (Teo *et al*., 2010; Kim *et al*., 2011). *gskA*$^-$ cells were reported to have reduced production of the PI3K product phosphatidylinositol (3,4,5)-triphosphate (PI(3,4,5)$P_{3)}$ and reduced phosphorylation of the activation loop (AL) of Akt/PKB and the related kinase PKBR1 (Teo *et al*., 2010).

To obtain more insight into the mechanisms by which Ras and Rap1 control chemotaxis, we performed a bioinformatics screen for proteins with potential Ras/Rap1 binding domains and identified Daydreamer (DydA), a member of the Mig10/RIAM/lamellipodin (MRL) family of adaptor proteins, as a new Ras/Rap1 effector. We show that DydA localizes to the leading edge of chemotaxing cells and plays key roles in regulating both F-actin polymerization and myosin II (MyoII) assembly, in part by regulating the kinetics of Akt/PKB and the related enzyme PKBR1. We found that DydA binds RasG-GTP and is phosphorylated by GSK-3 and that this phosphorylation is required for some of DydA's functions. Through a detailed analysis of the g*skA*$^-$ cell chemotactic phenotype, we demonstrate that the kinetics and levels of the activities of Ras, Akt/PKB, and PKBR1 are misregulated in *gskA*$^-$ cells. These studies link the Ras and GSK-3 signaling networks through the protein DydA and provide insights into how these networks regulate directional sensing and chemotaxis.

RESULTS

Daydreamer (DDB_G0287875) is required for proper chemotaxis

DDB_G0287875 was identified in a bioinformatics search of the *Dictyostelium* database for proteins that have Ras-association (RA) domains and thus represented a new, potential Ras and/or Rap1 effector. From its domain structure (Figure 1A), DDB_G0287875 appears to be a member of the MRL family of adaptor proteins that act downstream of Ras-like GTPases and translate extracellular signals into changes of the actin cytoskeleton affecting cell motility and adhesion (Krause *et al*., 2004; Lafuente *et al*., 2004; Chang *et al*., 2006; Lyulcheva *et al*., 2008). Like other MRL proteins, DDB_G0287875 has an N-terminal RA domain, followed by a pleckstrin homology (PH) domain and a proline-rich motif (PRM). In addition, DDB_G0287875 has two calponin homology (CH) domains (Friedberg and Rivero, 2009) and a second RA domain at the C-terminus. On the basis of the chemotactic defects of the DDB_G0287875 null strain described below, we have named the protein Daydreamer, or DydA.

To determine whether DydA plays a role in chemotaxis, we generated *dydA*$^-$ cells by homologous recombination and analyzed the chemotactic properties of these cells. *dydA*$^-$ cells exhibit strong chemotactic defects: when placed in a strong chemoattractant gradient emitted by a micropipette, *dydA*$^-$ cells polarize weakly, move with reduced speed and deeply reduced directionality, and have more lateral filopodia (Figure 1, B–D, and Supplemental Movies S1 and S2). In shallow, linear gradients produced in a Dunn chamber, the cells do not move (as noted in Figure 3C, which appears later in this article). The low, measured speed results from jiggling of the cells, which results in a change in the location of the cell's centroid. Because of the slow, more random, and lackadaisical "pace" of chemotaxis, we named the gene *daydreamer* (*dydA*).

Tagged DydA complements the *dydA*$^-$ cell chemotactic defects and DydA–green fluorescent protein (DydA-GFP) localizes to the leading edge of chemotaxing and randomly moving cells (Figure 1, C and E), suggesting that DydA is involved in leading-edge signaling. GFP-DydA also transiently localizes from the cytosol to the plasma membrane in response to uniform (global) chemoattractant stimulation with peak localization at ~7–9 s (Figure 1F). Pretreatment with latrunculin B, an inhibitor of F-actin polymerization, results in a high basal level of DydA at the cortex with no additional recruitment upon chemoattractant stimulation, suggesting that F-actin plays a role in regulating DydA's cortical localization (Figure 1G). *dydA*$^-$ cells exhibit a very elevated and extended first and second peak of F-actin polymerization and an extended and highly elevated second peak (Figure 1H). The level of assembled MyoII is elevated ~40% in unstimulated cells and, upon chemoattractant stimulation, the kinetics of MyoII are similar to those of wild-type cells (Figure 1I). These findings indicate that DydA plays a role in negatively regulating F-actin polymerization and MyoII assembly.

dydA$^-$ cells exhibit an extended and highly elevated plasma membrane localization of the PI(3,4,5)P_3 reporter PH_{crac} in response to chemoattractant stimulation (Figure 2A), suggesting that PI3K activity is elevated and extended. As elevated levels of PIP3 can result in dominant, gain-of-function phenotypes that result in multiple pseudopod formation, we tested whether addition of the PI3K inhibitor LY294002 suppressed the *dydA*$^-$ chemotactic phenotype and found that it did not (unpublished data). We also examined the regulation and activity of Akt/PKB and the related enzyme PKBR1, both of which play key roles in regulating leading-edge function during chemotaxis (Meili *et al*., 1999, 2000; Kamimura *et al*., 2008). Akt/PKB and PKBR1 are activated at the plasma membrane by two phosphorylations, as are mammalian Akt/PKBs (Sarbassov *et al*., 2005): the ALs are phosphorylated by the two PDK1 isoforms, PdkA and PdkB (Kamimura *et al*., 2008; Liao *et al*., 2010), while TORC2 phosphorylates the conserved hydrophobic motif (HM) of Akt/PKB and PKBR1 (Lee *et al*., 2005; Kamimura *et al*., 2008; Cai *et al*., 2010; Liao *et al*., 2010). Chemoattractant-mediated plasma membrane localization of Akt/PKB is mediated through the binding of the PH domain of Akt/PKB to the PI3K product PI(3,4,5)P_3 (Meili *et al*., 1999;

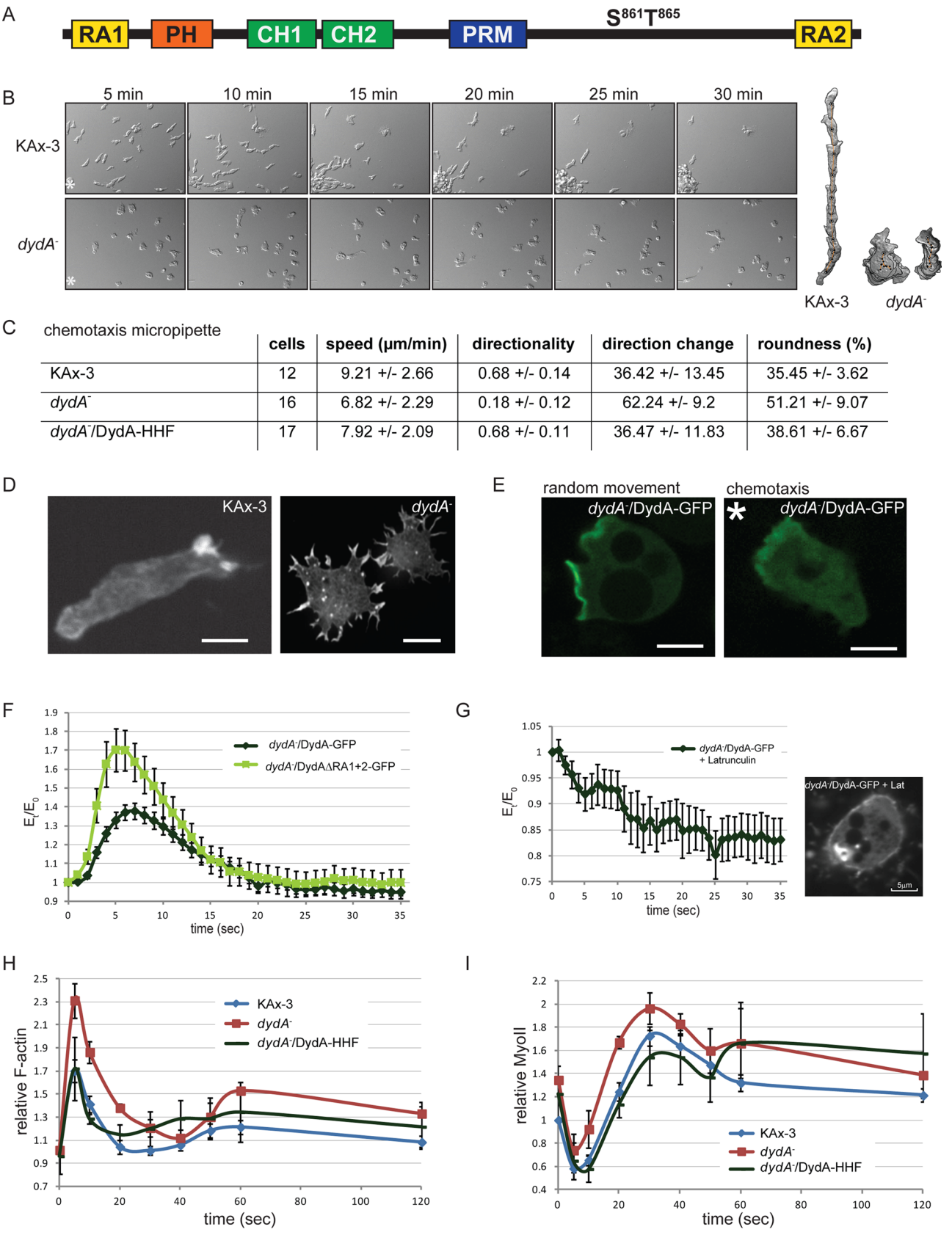

C

chemotaxis micropipette

	cells	speed (µm/min)	directionality	direction change	roundness (%)
KAx-3	12	9.21 +/- 2.66	0.68 +/- 0.14	36.42 +/- 13.45	35.45 +/- 3.62
dydA⁻	16	6.82 +/- 2.29	0.18 +/- 0.12	62.24 +/- 9.2	51.21 +/- 9.07
dydA⁻/DydA-HHF	17	7.92 +/- 2.09	0.68 +/- 0.11	36.47 +/- 11.83	38.61 +/- 6.67

FIGURE 1: *dydA*⁻ cells exhibit chemotactic defects. (A) Domain structure of DDB_G0287875/Daydreamer. RA, Ras association domain; PH, pleckstrin homology domain; CH, calponin homology domain; PRM, proline-rich motif; S^{861} and T^{865}, phosphorylated residues. (B) Live imaging of chemotaxing wild-type and *dydA*- cells. The source of the chemoattractant is located in the lower left corner of the images; images are at 5-min intervals over a 30-min time frame. (C) DIAS analysis of wild-type cells, *dydA*⁻ cells, and *dydA*⁻ cells expressing DydA-HHF chemotaxing toward a

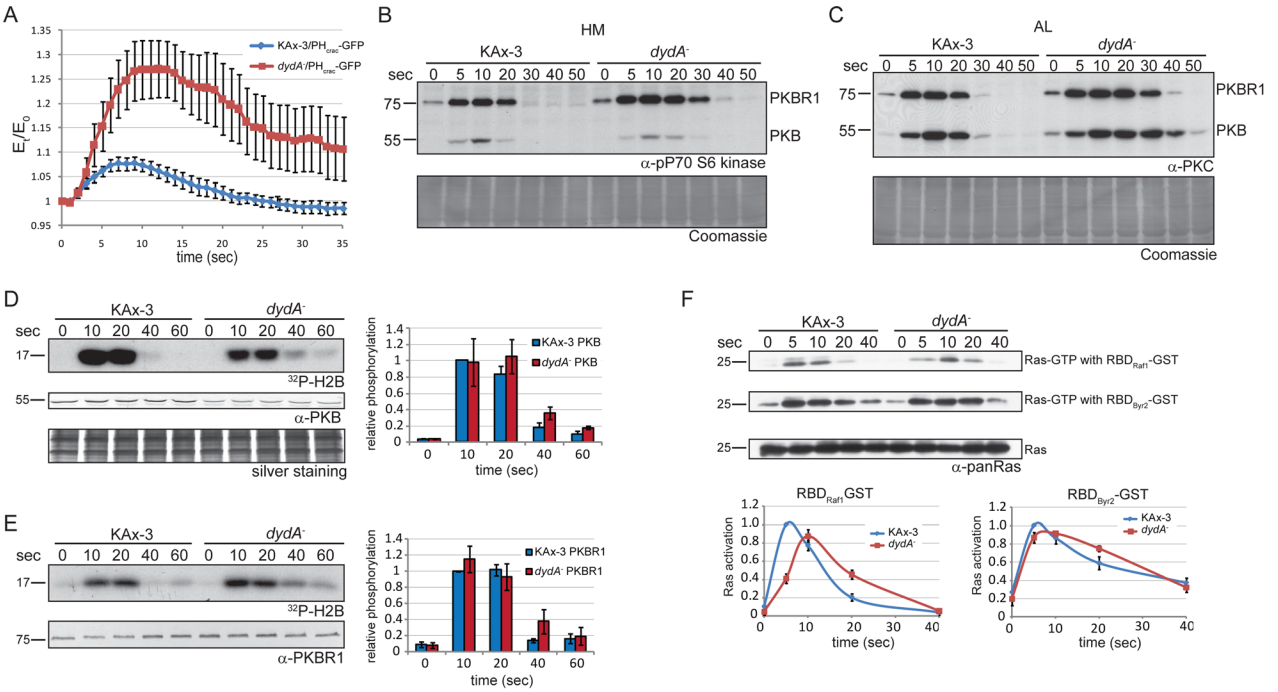

FIGURE 2: Lack of DydA affects Ras effector pathways. (A) Translocation kinetics of PH$_{crac}$-GFP in *dydA*$^-$ cells in response to cAMP stimulation. Data represent mean ± SE of relative fluorescence intensity of membrane-localized PH$_{crac}$-GFP as a function of time after cAMP stimulation with the starting condition taken as 1.0. (B and C) Phosphorylation of the HM and AL, respectively, of Akt/PKB and PKBR1 in wild-type and *dydA*$^-$ cells in response to cAMP. Coomassie Blue staining was used as loading control. (D and E) cAMP-induced Akt/PKB and PKBR1 kinase activity, respectively. H2B was used as substrate; protein levels were determined by immunoblotting and silver staining was used as loading control; for quantification, the maximum value of wild-type cells was taken as 1.0; data are mean ± SE of at least three independent experiments. (F) Ras activation in *dydA*$^-$ cells. cAMP-induced Ras activation was assessed using RBD$_{Raf1}$ and RBD$_{Byr2}$ in pull-down assays; levels of total Ras and Ras-GTP were analyzed with panRas immunoblotting and quantified, with the maximum value of wild-type cells was taken as 1.0; data are mean ± SD of at least three independent experiments.

Funamoto *et al.*, 2002), while PKBR1 is constitutively localized on the plasma membrane through an N-terminal myristoyl group and does not require either PI3K activity or PI(3,4,5)P$_3$ binding for its activation (Meili *et al.*, 2000; Lee *et al.*, 2005; Kamimura *et al.*, 2008). In wild-type cells, under our experimental conditions, the AL and HM phosphorylation of Akt/PKB and PKBR1 peak at ~10 s after chemoattractant stimulation, consistent with the peak of kinase activity (Figure 2, B–E; quantitation of the data in Figure 2, B and C, is presented in Supplemental Figure S1A; Meili *et al.*, 1999, 2000; Lee *et al.*, 2005). In *dydA*$^-$ cells, we observe that the HM phosphorylation is elevated for Akt/PKB and PKBR1 and that the phosphorylation of the AL is elevated and extended. Although the relative specific activity of Akt/PKB kinase activity is similar to that in wild-type cells, the total level of Akt/PKB protein and kinase activity is ~50% that of wild-type cells. The greatest effect of *dydA*$^-$ cells is on the AL phosphorylation of Akt/PKB, consistent with elevated levels of PI(3,4,5)P$_3$ activity.

Role of the RA domains in controlling DydA function

The small GTPases Ras and Rap1 are major regulators of chemotaxis and lie upstream from PI3K and TORC2 (Lee *et al.*, 1999; Funamoto *et al.*, 2002; Sasaki *et al.*, 2004, 2007; Sasaki and Firtel, 2006; Bolourani *et al.*, 2006, 2008; Charest *et al.*, 2010). As DydA has two RA domains, we examined the possible role of DydA on the

micropipette emitting cAMP. Data represent mean ± SD; speed indicates the speed of the cells' centroid movement along the total path; directionality indicates the linearity of the migration paths; direction change is a relative measure of the number and frequency of turns of the cells; roundness is a measure of the polarization of the cells. (D) F-actin localization in wild-type and *dydA*$^-$ aggregation-competent (developed) cells using fluorescent phalloidin. Scale bar: 10 μm. (E) Localization of DydA-GFP in vegetative randomly moving cells and aggregation-competent chemotaxing cells. Asterisk indicates the chemoattractant source. (F) Translocation kinetics of DydA-GFP and DydAΔRA1+2-GFP in response to cAMP stimulation. The data represent the mean ± SE of relative fluorescence intensity of membrane-localized DydA-GFP as a function of time after cAMP stimulation with the starting condition taken as 1.0. (G) Translocation kinetics of DydA-GFP in response to cAMP stimulation after latrunculin B treatment. The data represent the mean ± SE of relative fluorescence intensity of membrane-localized DydA-GFP as a function of time after cAMP stimulation, with the starting condition taken as 1.0. (H) cAMP-induced F-actin polymerization. Data represent mean ± SE of at least three independent experiments, with the starting condition in wild-type cells taken as 1.0. (I) cAMP-induced MyoII assembly. Data represent mean ± SE of at least three independent experiments, with the starting condition in wild-type cells taken as 1.0.

activation of Ras and Rap1. Ras activation was quantitated using pull-down assays employing two Ras-binding domains (RBDs) with different binding specificities: the Raf1-RBD (RBD_{Raf1}), which preferentially binds RasG, RasD, and RasB, and the Byr2-RBD (RBD_{Byr2}), which preferentially binds RasC and, with a lower affinity, RasG (Kae *et al*., 2004; Zhang *et al*., 2008). As previously reported (Kae *et al*., 2004; Sasaki *et al*., 2004; Zhang *et al*., 2008; Charest *et al*., 2010), using RBD_{Raf1}, we found that wild-type cells exhibit a low basal level of Ras-GTP, which rises rapidly in response to chemoattractant stimulation with a peak at ~5 s and then returns quickly to basal levels. In contrast, the activity measured using RBD_{Byr} peaks at ~10 s (Figure 2F). This difference in the observed Ras activation kinetics in wild-type cells using the RBD_{Raf1} versus the RBD_{Byr2} probe is consistent with previous findings that RasG activation peaks at ~5 s, whereas RasC peaks at ~10 s (Kae *et al*., 2004; Sasaki *et al*., 2004; Zhang *et al*., 2008). Surprisingly, in *dydA*$^-$ cells, Ras activation using the RBD_{Raf1} probe is not increased, but is slightly decreased and delayed (Figure 2F), suggesting that the cause for the greatly extended and elevated cortical localization of PH_{crac} is independent of the level of Ras activation. Ras activity as measured using RBD_{Byr2} is unaltered in *dydA*$^-$ cells compared with that in wild-type cells. Similarly, we found chemoattractant-mediated Rap1 activation to be unaltered in these cells (Figure S1B).

To determine whether the DydA RA domains bind Ras and/or Rap1, similar to RA domains of other MRL members (Lafuente *et al*., 2004), we expressed RA1 and RA2 as GFP fusions in wild-type cells and used the glutathione *S*-transferase (GST) fusions of the GDP and GTP forms of RasG, RasC, and Rap1 (RapA), and found that GFP-RA1 was only pulled down by RasG-GTPγS from *Dictyostelium* cell lysates (Figure 3A). We also did not observe binding of the activated form of Rap1 with a DydA fragment containing RA1 and the adjacent PH domain (unpublished data). None of the Ras proteins pulled down GFP-RA2. We also examined the ability of the activated (GppNHp-bound) form of recombinant GST-RasC, -RasG, -RasD, which is closely related to RasG, and -Rap1 to bind recombinant RA1 and RA2 and found that only RasG- GppNHp and RasD-GppNHp showed any detectable binding (Figure S1C). Finally, we examined the ability of recombinant RA1 to stimulate the dissociation of mGppNHp from RasG, an assay of RA1 binding to RasG-GTP. In agreement with our other data indicating RasG-GTP binds RA1, we show that RA1 has GDI activity by demonstrating that addition of RA1 inhibits the dissociation of 2′/3′-O-(N-Methylanthraniloyl)-guanosine-5′-[(β,γ)-imido]triphosphate (mGppNHP) from RasG and that the inhibition depends upon the concentration of RA1 (Figure S1D). As RasG is expressed throughout growth and aggregation, and RasD is preferentially expressed during multicellular development (Reymond *et al*., 1984; Robbins *et al*., 1989), we suggest that RasG is the major Ras protein that binds to DydA through RA1. We cannot exclude that another Ras protein we have not tested may interact with either RA domain.

To further understand the role of the two RA domains, we examined the phenotypes of *dydA*$^-$ cells expressing His-hemagglutinin-FLAG (HHF)-tagged DydA lacking both RA domains (DydAΔRA1+2-HHF) and found that the cells exhibit strong chemotactic phenotypes, indicating that the RA domains are required for DydA function. In a steep gradient emitted by a micropipette, the cells are less polarized and move slightly more slowly than wild-type cells. In a shallow, linear gradient produced in a Dunn chamber (Zicha *et al*., 1991), the cells are unable to migrate and the phenotype is as severe as that observed for *dydA*$^-$ cells (Figure 3, B and C). When we analyzed the profile of F-actin polymerization and MyoII assembly in *dydA*$^-$ cells expressing DydAΔRA1+2-HHF, we found that both peaks of F-actin polymerization are reduced compared with wild-type cells and that the first peak of actin decreases much faster than in wild-type cells (Figure 3D). This suggests that DydAΔDRA1+2 inhibits F-actin polymerization and facilitates F-actin depolymerization. We also found that MyoII assembly is dramatically reduced in *dydA*$^-$/DydAΔRA1+2 cells compared with wild-type cells (Figure 3E). These findings were unexpected, as *dydA*$^-$ cells show elevated basal levels of assembled MyoII but normal kinetics and levels of chemoattractant-mediated assembly, suggesting that DydAΔRA1+2, directly or indirectly, inhibits MyoII assembly and F-actin polymerization. In addition, we found that the phosphorylations of the HM and AL sites of Akt/PKB and PKBR1 are extended, as is the case for *dydA*$^-$ cells (Figure 3, F and G, and quantitation in Figure S1A). DydAΔRA1+2-GFP localizes to the leading edge of chemotaxing cells (Movie S3). Interestingly, DydAΔRA1+2-GFP exhibits a highly elevated level of cortical localization upon chemoattractant stimulation but with response kinetics similar to those of wild-type cells (Figure 1F). These observations, together with the fact that the activity of Ras and Rap1 is not severely altered in *dydA*$^-$ cells, suggest that DydA might act as a downstream effector of Ras that directly or indirectly regulates F-actin polymerization and MyoII assembly. Furthermore, the RA domains are required for modulating the regulation of DydA function but not its localization per se.

The CH domains and the PRM, but not the PH domain, are involved in localizing DydA to the leading edge

The MRL family member lamellipodin is recruited to the leading edge of fibroblasts upon platelet-derived growth factor (PDGF) stimulation through the interaction of its PH domain with phosphatidylinositol (3,4)-bisphosphate ($PI(3,4)P_2$; Krause *et al*., 2004). As DydA localizes to the leading edge of chemotaxing *Dictyostelium* cells, we tested whether this localization requires the PH domain of DydA. We found that DydAΔPH-GFP still localizes to the leading edge of migrating cells, translocates to the membrane upon global stimulation with kinetics similar to DydA-GFP, and complements the *dydA*$^-$ cells' chemotactic phenotypes, indicating the PH domain is not required (Figures 3, H and I, and S1F). We used the PH domain of DydA in a lipid-binding assay and found that it predominantly binds phosphatidylinositol 3-phosphate (PI(3)P), a phospholipid predominantly found in endosomes and phagosomes, but not $PI(3,4)P_2$ or $PI(3,4,5)P_3$, products of class I PI3Ks (Figure S1E). We also found that treatment of *dydA*$^-$ cells expressing GFP-DydA with the PI3K inhibitor LY294002 does not block GFP-DydA recruitment to the plasma membrane, indicating that PI3K is not required for the recruitment to the plasma membrane (unpublished data).

Interestingly, the stimulus-dependent cortical translocation of DydA was delayed and reduced in the absence of both CH domains (*dydA*$^-$/DydAΔCH1+2-GFP; Figure 3I), indicating a function of the CH domains in DydA's cortical localization. The deletion of both CH domains causes defects during chemotaxis: in a steep gradient, the cells move with a slightly higher speed than wild-type cells, but they turn more often than wild-type cells, and we observed an increase in bifurcated pseudopodia (Figure S1C), a phenotype that has been reported for mutants of the SCAR/WAVE complex (Blagg *et al*., 2003). *dydA*$^-$/DydAΔCH1+2-HHF cells exhibit an extended F-actin first peak and an elevated second peak (Figure 3D). These cells also exhibit an elevated basal level of assembled MyoII and kinetics similar to those of *dydA*$^-$ cells (Figure 3E), suggesting the CH domains are important in modulating the levels of F-actin and assembled MyoII.

In addition to the CH domains, the PRM plays a role in the cortical localization of DydA in response to a chemoattractant stimulus.

DydAΔPRM-GFP shows reduced localization to the cortex in response to chemoattractant stimulation, and *dydA*$^-$ cells expressing DydAΔPRM-HHF show reduced migration speed (Figures 3I and S1C); a deletion of the CH domains together with the PRM domain further reduces the localization of the protein to the cortex and the leading edge (Figure 3I), indicating that these domains contribute to the localization of DydA to the leading edge but are not solely responsible for DydA's subcellular localization. The PRM from the mammalian MRL member lamellipodin binds VASP, which is required for lamellipodin function. We tested whether the DydA PRM binds to *Dictyostelium* VASP in a pull-down assay and were unable to detect any binding (unpublished data). Furthermore, unlike the PRM of lamellipodin, which has a sequence context similar to that of other VASP-binding PRM domains, the sequence of the DydA PRM does not. Taken together, our findings indicate that the CH and PRM domains, but not the PH domain, contribute to the localization of DydA to the leading edge of chemotaxing cells and are important for the function of DydA in regulating the cytoskeleton.

GSK-3 phosphorylates DydA and is required for some, but not all, DydA functions

We previously reported using total-cell phosphoproteomic analysis of unstimulated (0 s, basal) cells and cells stimulated for 10 s (the time of maximum activation of many leading-edge pathways) and 60 s (adaptation) to identify proteins that are differentially phosphorylated in response to chemoattractant stimulation (Charest *et al.*, 2010). These phosphoproteomic data indicated that in wild-type cells, DydA is constitutively phosphorylated at Ser$^{860/861}$ and Thr^{865}, which lie between the PRM and the C-terminal RA2 domain (Figure 1A; unpublished data). Treatment of DydA-HHF purified from *dydA*$^-$ cells with λ-protein phosphatase results in an increase in DydA-HHF mobility on SDS gels, consistent with the protein being phosphorylated (Figure 4A).

The identified phosphorylation site in DydA matches the GSK-3 consensus motif Ser/Thr-(X-X-X)-pSer/pThr, with X being any amino acid (Figure 4B). GSK-3 has a unique substrate specificity wherein, for efficient phosphorylation by GSK-3, many substrates require a Ser/Thr priming phosphorylation at a site located four residues C-terminal to the site of GSK-3 phosphorylation, with both the priming phosphorylation and the phosphorylation by GSK-3 often being Pro-directed (Ser/Thr-(Pro-X-X)-pSer/pThr-Pro; Frame *et al.*, 2001). As the DydA phosphorylation site conforms to a GSK-3 consensus site with both sites followed by a Pro (Figure 4B), we repeated the whole-cell phosphoproteomic analysis of wild-type cells and, at the same time, cells lacking GSK-3 (*gskA*$^-$ cells) before and at 10 and 60 s after chemoattractant stimulation. When compared with wild-type cells, the phosphorylation of DydA at the GSK-3 site in *gskA*$^-$ cells is dramatically reduced, which is consistent with a decrease in the mobility of DydA-HHF purified from *gskA*$^-$ cells compared with that from *dydA*$^-$ cells (wild-type for *gskA*) on SDS gels (Figure 4, C and D).

To verify that DydA is a direct target of GSK-3, we expressed DydA-HHF in *gskA*$^-$ cells, immunoprecipitated the tagged protein, and used it in an in vitro kinase assay with recombinant human GSK-3β. Figure 4D illustrates that DydA can be directly phosphorylated by GSK-3β in vitro. Phosphorylation data on DydA carrying Ala mutations of Ser^{860} or Ser^{861} together with Thr^{865} indicate that Ser^{861} is the residue that is preferentially phosphorylated by GSK-3β, which is consistent with the consensus site for GSK-3 (Figure 4D). Unexpectedly, DydA-HHF in which three Ser residues (Ser$^{859–861}$) are mutated to Ala exhibits moderate phosphorylation (Figure 4D). A possible explanation for this observation might be that these mutations lead to changes that make the adjacent Ser highly accessible for GSK-3β. The in vitro kinase assay, together with the phosphoproteomic findings, suggests that DydA is a direct target for GSK-3 in vivo. Interestingly, we observed some phosphorylation of DydA in *gskA*$^-$ cells (Figure 4, C and D). The phosphorylation occurs to a very small extent in the GSK-3 consensus motif, but mainly on adjacent Ser/Thr residues (see *Discussion*).

To examine the importance of phosphorylation by GSK-3 for the function of DydA, we expressed the nonphosphorylatable form of Daydreamer (DydA$^{S861A/T865A}$-HHF) in *dydA*$^-$ cells. In a steep chemotactic gradient, these cells migrate more slowly than wild-type cells, but the defects are less severe than in the *dydA*$^-$ cells (Figure 4E). However, in a shallow, linear gradient, these cells do not migrate at all and the defects are as strong as those of *dydA*$^-$ cells (Figure 4F), indicating that phosphorylation of DydA by GSK-3 plays an important role for the function of DydA during chemotaxis. Like *dydA*$^-$ cells, *dydA*$^-$ cells expressing DydA$^{S861A/T865A}$-HHF exhibit increased MyoII assembly upon chemoattractant stimulation (Figure 3E). The elevated and extended phosphorylation of the AL and HM motifs of Akt/PKB and PKBR1 exhibited by *dydA*$^-$ cells is only partially suppressed by expressing DydA$^{S861A/T865A}$-HHF, while the elevated F-actin response is fully suppressed (Figures 3, D, F, and G, and S1A). These observations suggest that some, but not all, functions of Daydreamer require phosphorylation by GSK-3. We tried to generate a phosphomimic version of DydA by mutating Ser^{861} to Glu and Thr^{865} to Asp. Expression of DydA$^{S861E/T865D}$-HHF in *dydA*$^-$ cells does not complement *dydA*$^-$ phenotypes but produces dominant effects: wild-type as well as *dydA*$^-$ cells expressing DydA$^{S861E/T865D}$ exhibit deeply reduced speed and lower directionality (unpublished data).

gskA$^-$ cells exhibit strong chemotactic defects

As DydA requires phosphorylation by GSK-3 for full function, we wanted to understand the role of GSK-3 in context with GSK-3's overall role in chemotaxis. To this end, we conducted an analysis of the phenotype of *gskA*$^-$ cells similar to that which we performed on *dydA*$^-$ cells. Consistent with previously reported observations, we found that *gskA*$^-$ cells exhibit strong chemotactic defects (Teo *et al.*, 2010; Kim *et al.*, 2011; Figure 5, A and B, and Movies S4 and S5). The cells are less polarized, show a reduced speed compared with wild-type cells, lack directionality in their migration, and move almost randomly in a chemoattractant gradient emitted by a micropipette. These defects are more severe than those of *dydA*$^-$ cells. During development, *gskA*$^-$ cells form small aggregates through random collision and adhesion rather than directed migration toward each other (Figure S2A). The migration parameters of developed, "aggregation-competent" *gskA*$^-$ cells migrating in a chemoattractant gradient are similar to those of cells moving randomly in the absence of a chemoattractant gradient (Figure 5A), suggesting that GSK-3 has an important role in gradient sensing rather than cell motility and/or linking directional sensing with persistent, localized F-actin polymerization at the site on the cortex closest to the chemoattractant source. In addition, the analysis of random movement of vegetative cells demonstrates that *gskA*$^-$ vegetative cells move faster than wild-type cells (Figure 5C), suggesting that the lack of efficient chemotaxis of *gskA*$^-$ cells is not due to defects in motility.

The level of F-actin polymerization in *gskA*$^-$ cells is similar to that of wild-type cells, but the first peak decreases faster than in wild-type cells (Figure 5D). However, the level of MyoII assembly upon chemoattractant stimulation is reduced dramatically in *gskA*$^-$ cells (Figure 5E). Interestingly, the rapid decrease of the first peak of F-actin and the dramatic reduction in MyoII assembly are also observed in *dydA*$^-$ cells expressing DydAΔRA1+2-HHF. Because MyoII assembly is

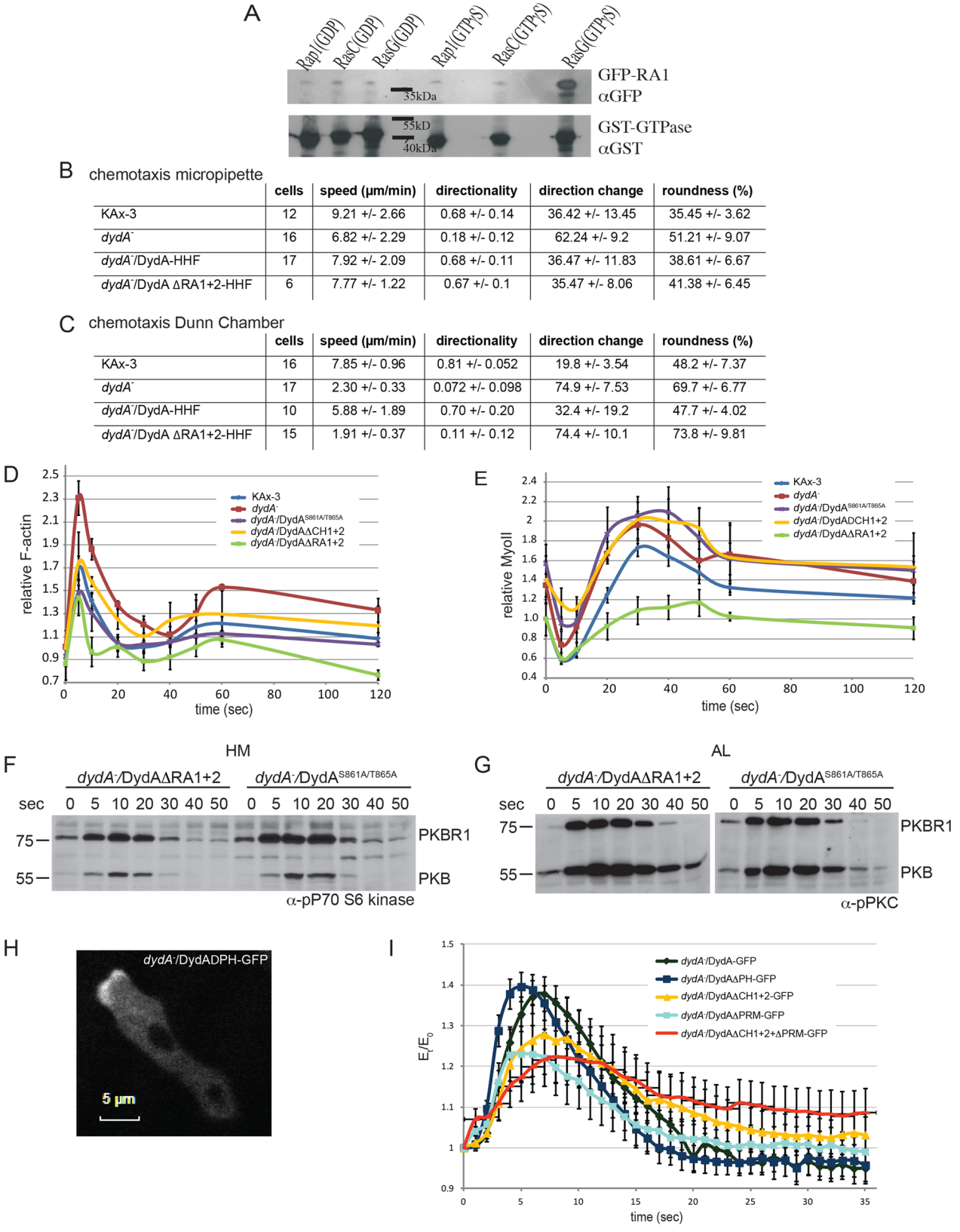

B chemotaxis micropipette

	cells	speed (µm/min)	directionality	direction change	roundness (%)
KAx-3	12	9.21 +/- 2.66	0.68 +/- 0.14	36.42 +/- 13.45	35.45 +/- 3.62
dydA⁻	16	6.82 +/- 2.29	0.18 +/- 0.12	62.24 +/- 9.2	51.21 +/- 9.07
dydA⁻/DydA-HHF	17	7.92 +/- 2.09	0.68 +/- 0.11	36.47 +/- 11.83	38.61 +/- 6.67
dydA⁻/DydA ΔRA1+2-HHF	6	7.77 +/- 1.22	0.67 +/- 0.1	35.47 +/- 8.06	41.38 +/- 6.45

C chemotaxis Dunn Chamber

	cells	speed (µm/min)	directionality	direction change	roundness (%)
KAx-3	16	7.85 +/- 0.96	0.81 +/- 0.052	19.8 +/- 3.54	48.2 +/- 7.37
dydA⁻	17	2.30 +/- 0.33	0.072 +/- 0.098	74.9 +/- 7.53	69.7 +/- 6.77
dydA⁻/DydA-HHF	10	5.88 +/- 1.89	0.70 +/- 0.20	32.4 +/- 19.2	47.7 +/- 4.02
dydA⁻/DydA ΔRA1+2-HHF	15	1.91 +/- 0.37	0.11 +/- 0.12	74.4 +/- 10.1	73.8 +/- 9.81

FIGURE 3: Role of the DydA domains in controlling DydA function. (A) Pull down in *Dictyostelium* lysate with the indicated inactive (GDP) or active (GTP) bound GST-GTPase as bait and GFP-DydRA1 as prey. The amount of prey and bait (bottom panel) were detected by Western blotting using antibody specific for GFP or GST, respectively. (B and C) DIAS analysis of chemotaxis of *dydA*⁻ and wild-type cells in response to a chemoattractant gradient produced by a micropipette (B) or in a Dunn chamber (C). Data represent mean ± SD; speed indicates the speed of the cells' centroid movement along the total path; directionality indicates the linearity of the migration paths; direction change is

regulated by Rap1 (Kortholt *et al.*, 2006; Jeon *et al.*, 2007), we analyzed the activation of Rap1 using RBD_{RalGDS} in pull-down assays and observed a slight increase in the basal level of activated Rap1 and a slightly lower level of Rap1 activation on stimulation in *gskA*$^-$ cells compared with wild-type cells (Figure S2B). But these slight differences cannot account for the dramatic reduction of MyoII assembly observed in the *gskA*$^-$ cells. This indicates that GSK-3 affects MyoII assembly mainly downstream from or independent of Rap1, possibly through DydA, which also regulated MyoII assembly.

Because of the strong directionality defects exhibited by *gskA*$^-$ cells, we examined the activity of Ras using the two RBDs with different binding specificities, RBD_{Raf1} and RBD_{Byr2}, as described for DydA. Compared with wild-type cells, the kinetics of Ras activation using RBD_{Raf1} are delayed and extended in *gskA*$^-$ cells, with a broader peak centering at 10–20 s and with high levels of Ras-GTP still present at 30 s (Figure 6A). In contrast, when using RBD_{Byr2}, we found that the basal level of Ras-GTP was highly elevated and increased only slightly upon stimulation to the wild-type level and then decreased slowly to the high basal level observed in unstimulated *gskA*$^-$ cells, indicating a misregulation of Ras levels and kinetics in *gskA*$^-$ cells. This is in sharp contrast to *dydA*$^-$ cells, which show almost normal Ras regulation.

As discussed in the DydA Ras analysis, of the tested Ras proteins, RasC-GTP preferentially binds to RBD_{Byr2}, suggesting the elevated Ras-GTP levels assayed using the RBD_{Byr2} probe are due to elevated RasC-GTP. We tested this directly by expressing epitope-tagged RasC in wild-type and *gskA*$^-$ cells and assaying the kinetics and relative levels of RasC-GTP. Unexpectedly, we found that the normalized level of RasC activation was slightly lower in *gskA*$^-$ compared with that in wild-type cells. We suggest that the elevated Ras activation assayed by the RBD_{Byr2} probe is a different Ras and one that has not been previously characterized.

Because the kinetics of Ras activation in *gskA*$^-$ cells are highly aberrant, we investigated two known Ras effectors, TORC2 and PI3K, by analyzing the phosphorylation of the HM and AL of Akt/PKB and PKBR1. Compared with our observations in wild-type cells, both Akt/PKB and PKBR1 have a delayed peak and extended kinetics of HM phosphorylation in *gskA*$^-$ cells (Figures 6B and S2C). The phosphorylation of the AL is extended in Akt/PKB and PKBR1, with the effect being most pronounced on the Akt/PKB AL (Figures 6B and S2C). Akt/PKB shows a highly increased basal phosphorylation of the AL. We see a corresponding higher basal activity for the Akt/PKB kinase and greatly extended chemoattractant-mediated activation of Akt/PKB and PKBR1 kinase activity (Figure 6, C and D). These findings are in conflict with the results of Teo *et al.* (2010), who observed no phosphorylation of the AL of Akt/PKB and PKBR1 in *gskA*$^-$ cells. Our observations suggest that the regulation of Ras, Akt/PKB, and PKBR1 is highly aberrant in *gskA*$^-$ cells.

To determine whether the highly extended phosphorylation of the Akt/PKB AL is the result of elevated PI3K activity, which could result in an extended localization of Akt/PKB at the plasma membrane, we examined the kinetics and extent of plasma membrane localization of the $PI(3,4,5)P_3$-responsive reporter PH_{crac}-GFP. Unexpectedly, we found that PH_{crac}-GFP has a deeply reduced level of chemoattractant-stimulated membrane localization in *gskA*$^-$ compared with wild-type cells, but with the peak level remaining for a more extended time than that in wild-type cells (Figure 6E; Teo *et al.*, 2010). When we examined the kinetics of extent of chemoattractant-stimulated PI3K cortical localization using GFP-$PI3K_{loc}$ (a PI3K localization reporter, rather than full-length PI3K, which leads to elevated $PI(3,4,5)P_3$ levels and aberrant phenotypes [Funamoto *et al.*, 2002]), we found that, like the PI(3,4,5)P3 levels assayed using PH_{crac}-GFP, the proportion of PI3K that localized to the cortex was reduced, and the kinetics were extended (Figure 6F). These results indicate that changes in the phosphorylation of Akt/PKB in *gskA*$^-$ cannot be explained by increases in $PI(3,4,5)P_3$ levels or PI3K activity.

DISCUSSION

Role of DydA in regulating chemotaxis

We have identified DydA, a new member of the MRL family of adaptor proteins, and show that it is required for multiple regulatory pathways that control directional sensing and cell motility. *dydA*$^-$ cells move more slowly than wild-type cells in a steep chemoattractant gradient and with a significant reduction in directionality compared with that of wild-type cells. Thus DydA is required for both cell motility and directional sensing. In response to chemoattractant stimulation, a number of signaling pathways are activated normally in *dydA*$^-$ cells, indicating that the cells are not generally deficient in responding to chemoattractant. We suggest that DydA is required to efficiently amplify the chemoattractant gradient, as the cells exhibit significantly more severe defects in shallow than steep gradients. Because DydA is required for multiple chemotactic pathways, binds RasG-GTP via a domain required for its functions, and requires phosphorylation by GSK-3 for full function, we propose that DydA helps integrate the function of several signaling pathways to regulate cell polarity and chemotaxis.

The DydA RA1 domain binds RasG-GTP, but not RasC-GTP (another Ras required for chemotaxis in *Dictyostelium*), and DydA lacking RA1/2 is unable to complement *dydA*$^-$ phenotypes and results in dominant-negative phenotypes when expressed in wild-type cells. We are unable to test, and therefore directly demonstrate, that RasG activation is required for DydA, because of the strong phenotypes of rasG$^-$ and RasG-gain-of-function strains. However, as Ras activation is not greatly altered in *dydA*$^-$ cells, we suggest that DydA lies downstream of RasG-GTP. This result, combined with the requirement of the RA domains, is consistent with a model that DydA plays a key role in regulating RasG-mediated polarity and directionality. Furthermore, consistent with DydA's role in directional sensing, DydA localizes to the leading edge of migrating cells and rapidly and transiently to the cell cortex in response to chemoattractant stimulation in a process that requires, in part, the CH domains and the PRM. Although the RA domains are required for DydA function, they are not required to localize DydA to the cortex but may negatively modulate DydA cortical binding as DydA lacking these

a relative measure of the number and frequency of turns of the cells; roundness is a measure of the polarization of the cells. (D and E) cAMP-induced F-actin polymerization (D) and MyoII assembly (E). Data represent mean ± SE of at least three independent experiments, with the starting condition in wild-type cells taken as 1.0. (F and G) Phosphorylation of the HM and AL of Akt/PKB and PKBR1, respectively, in *dydA*$^-$ cells expressing DydAΔRA1+2-HHF or $DydA^{S861A/T865A}$–HHF in response to cAMP. Coomassie Blue staining was used as loading control. Quantification of normalized HM and AL phosphorylation of Akt/PKB and PKBR1 can be found in Figure S1A. (H) Localization of DydAΔPH-GFP at the leading edge. (I) Translocation kinetics of DydA-GFP carrying different deletions in response to cAMP stimulation. The data represent the mean ± SE of relative fluorescence intensity of membrane-localized DydA-GFP as a function of time after cAMP stimulation with the starting condition taken as 1.0.

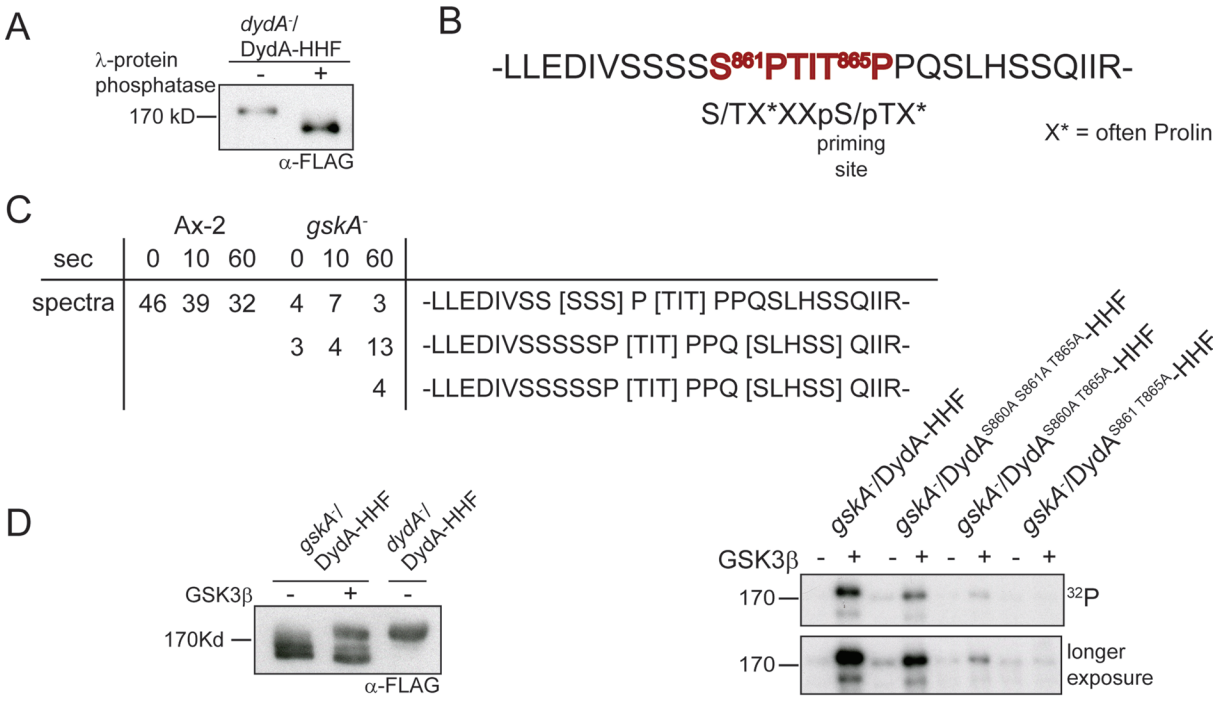

E chemotaxis micropipette

	cells	speed (µm/min)	directionality	direction change	roundness (%)
KAx-3	12	9.21 +/- 2.66	0.68 +/- 0.14	36.42 +/- 13.45	35.45 +/- 3.62
dydA-	16	6.82 +/- 2.29	0.18 +/- 0.12	62.24 +/- 9.2	51.21 +/- 9.07
dydA-/DydA-HHF	17	7.92 +/- 2.09	0.68 +/- 0.11	36.47 +/- 11.83	38.61 +/- 6.67
dydA-/DydA$^{S861A/T865A}$-HHF	8	7.5 +/- 0.97	0.63 +/- 0.12	39.99 +/- 7.77	33.39 +/- 3.84

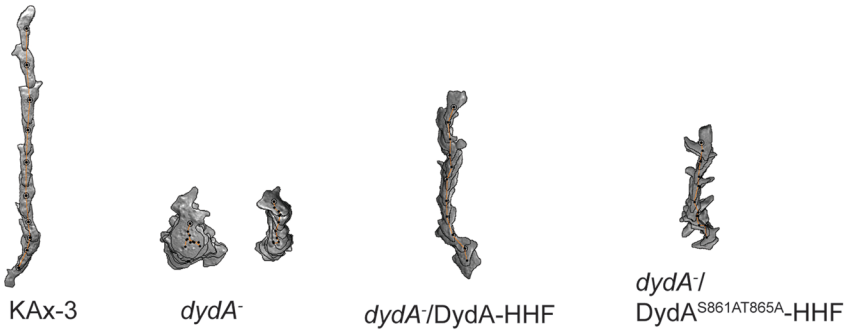

F chemotaxis Dunn Chamber

	cells	speed (µm/min)	directionality	direction change	roundness (%)
KAx-3	16	7.85 +/- 0.96	0.81 +/- 0.052	19.8 +/- 3.54	48.2 +/- 7.37
dydA-	17	2.30 +/- 0.33	0.072 +/- 0.098	74.9 +/- 7.53	69.7 +/- 6.77
dydA-/DydA-HHF	10	5.88 +/- 1.89	0.7 +/- 0.2	32.4 +/- 19.2	47.7 +/- 4.02
dydA-/DydA$^{S861A/T865A}$-HHF	17	2.02 +/- 0.25	0.043 +/- 0.041	80.7 +/- 5.88	72.0 +/- 5.84

FIGURE 4: Phosphorylation of DydA by GSK-3. (A) Phosphatase treatment of DydA-HHF. Phosphorylation of DydA from *dydA*⁻ cells was determined in the presence or absence of λ–protein-phosphatase. (B) Phosphorylation site of DydA and the GSK3 consensus motif. (C) Phosphoproteomic data of DydA in wild-type and *gskA*⁻ cells. Phosphorylation occurs in three different clusters of Ser/Thr. (D) In vitro kinase assay with DydA-HHF. Phosphorylation of DydA-HHF and DydA-HHF carrying Ala mutations in the GSK-3 consensus motif purified from *gskA*⁻ cells was examined in the presence and absence of GSK-3β. (E and F) DIAS analysis of chemotaxis of *dydA*⁻/DydA$^{S861A/T865A}$-HHF and control cells in response to a chemoattractant gradient produced by a micropipette (E) or in a Dunn chamber (F). Data represent mean ± SD; speed indicates the speed of the cells' centroid movement along the total path; directionality indicates the linearity of the migration paths; direction change is a relative measure of the number and frequency of turns of the cells; roundness is a measure of the polarization of the cells.

A

	chemotaxis		random movement	
	Ax-2	*gskA*⁻	Ax-2	*gskA*⁻
speed (μm/min)	10.32 +/- 1.97	6.12 +/- 1.95	3.53 +/- 1.53	6.04 +/- 2.97
directionality	0.74 +/- 0.07	0.26 +/- 0.21	0.28 +/- 0.1	0.33 +/- 0.2
direction change (deg)	29.15 +/- 6.73	46.83 +/- 9.71	48.0 +/- 6.89	36.24 +/- 11.28
roundness (%)	29.14 +/- 2.78	50.82 +/- 5.89	51.11 +/- 7.53	50.66 +/- 7.23

B

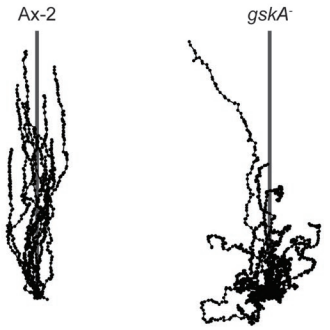

C

	vegetative cell motility	
	Ax-2	*gskA*⁻
speed (μm/min)	4.15 +/- 1.68	8.99 +/- 1.54
directionality	0.38 +/- 0.19	0.29 +/- 0.12
direction change (deg)	33.06 +/- 8.36	32.14 +/- 6.77
roundness (%)	51.39 +/- 5.26	47.8 +/- 3.99

D

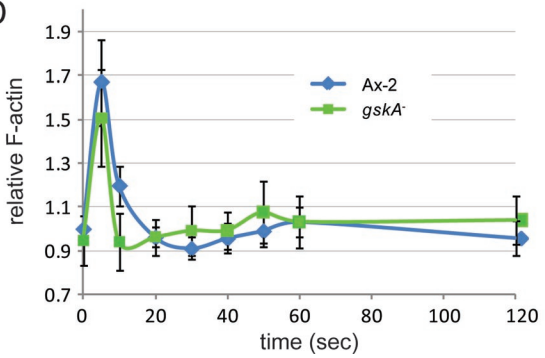

E

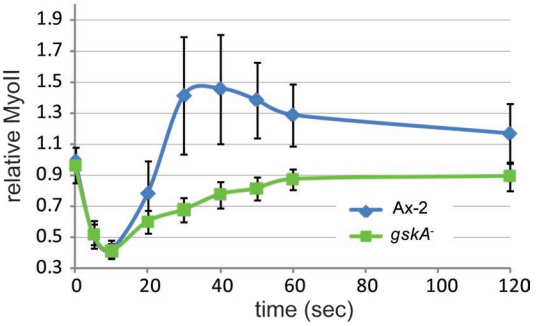

FIGURE 5: *gskA*⁻ cells exhibit severe chemotactic defects. (A) DIAS analysis of chemotaxing and randomly moving aggregation-competent wild-type and *gskA*⁻ cells. Data represent mean ± SD; speed indicates the speed of the cells' centroid movement along the total path; directionality indicates the linearity of the migration paths; direction change is a relative measure of the number and frequency of turns of the cells; roundness is a measure of the polarization of the cells. (B) Trajectories of cells moving toward cAMP. The plot represents the angle between the start and the end point of a cell relative to the chemoattractant gradient, represented by the vertical line. (C) DIAS analysis of randomly moving vegetative cells. Data represent mean ± SD; speed indicates the speed of the cells' centroid movement along the total path; directionality indicates the linearity of the migration paths; direction change is a relative measure of the number and frequency of turns of the cells; roundness is a measure of the polarization of the cells. (D and E) cAMP-induced F-actin polymerization and MyoII assembly, respectively, in *gskA*⁻ cells. Data represent the mean ± SE of at least three independent experiments, with the starting condition in wild-type cells taken as 1.0.

domains exhibits a highly elevated cortical binding. We also observed an extended phosphorylation of the ALs of AKT/PKB and PKBR1, which is consistent with the extended activity of PI3K based on PH-domain localization studies. However, the relative levels and kinetics of chemoattractant-mediated kinase activity are only slightly extended compared with wild-type cells.

Our analyses indicate that DydA is required for the regulation of the cytoskeleton. *dydA*⁻ cells exhibit a highly elevated first and second peak of F-actin assembly. As the basal level of F-actin is similar to that seen in wild-type cells, we suggest that DydA functions to negatively regulate the extent of chemoattractant-mediated F-actin polymerization, although we have not demonstrated that this is a direct effect. This is in contrast to the MRL protein lamellipodin, which stimulates F-actin polymerization at the leading edge through the recruitment of VASP. We also found that the basal levels of MyoII are elevated in *dydA*⁻ cells. A direct role for DydA in F-actin polymerization and MyoII assembly downstream of Ras family GTPases is also supported by the considerable inhibition of both responses in *dydA*⁻ cells expressing DydAΔRA1+2. We suggest that DydAΔRA1+2 acts as an active form of DydA, binds to and blocks the function of DydA effectors, and inhibits the regulation of F-actin assembly and/or promotes faster F-actin depolymerization.

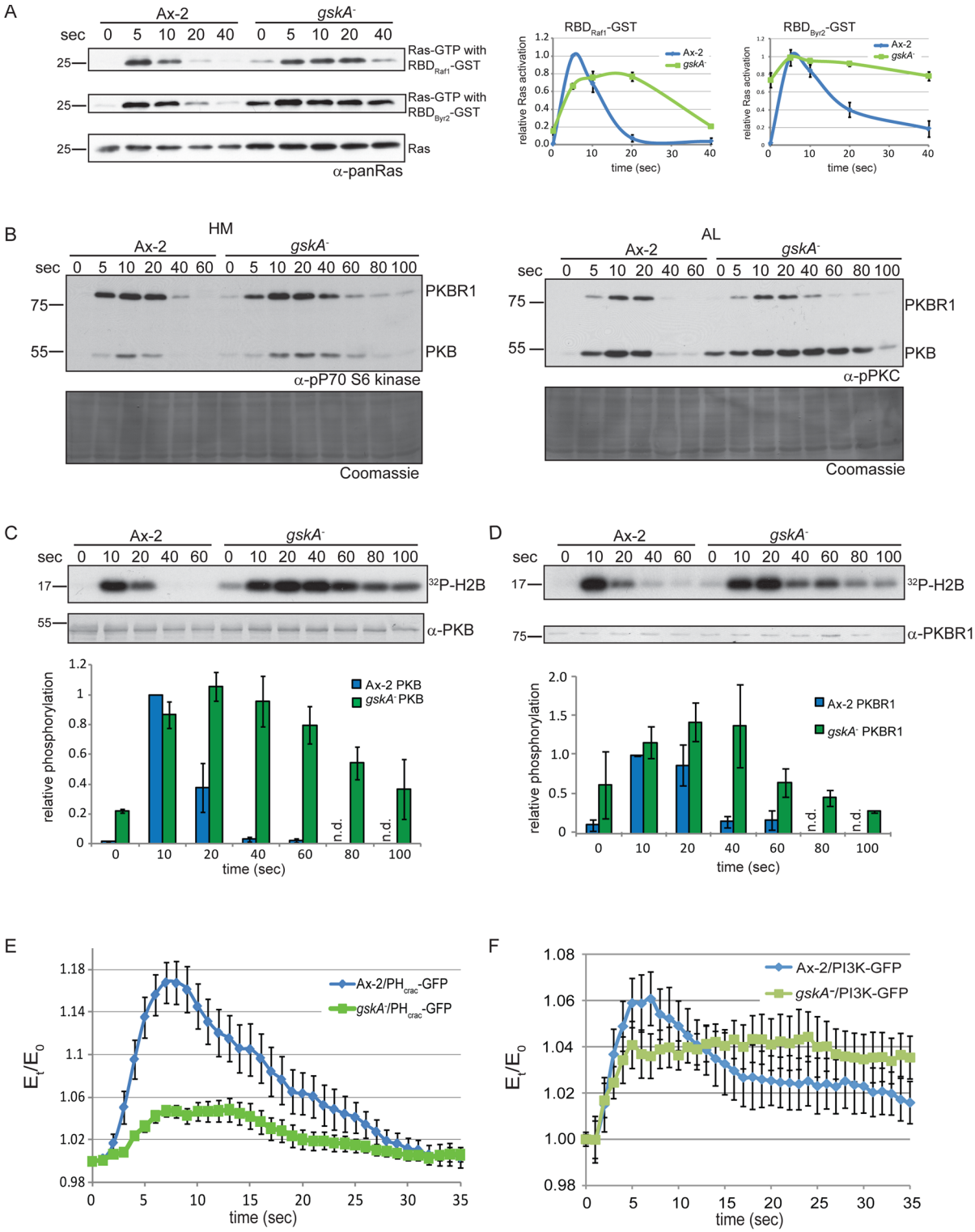

FIGURE 6: Regulation of effector pathways by GSK-3. (A) Ras activation in *gskA*⁻ cells. cAMP-induced Ras activation was assessed using RBD_{Raf1} and RBD_{Byr2} in pull-down assays. Levels of total Ras and Ras-GTP were detected by immunoblotting with an anti–pan-Ras antibody and quantified, with the maximum value of wild-type cells was taken as 1.0; data are mean ± SD of at least three independent experiments. (B) Phosphorylation of the HM and AL of Akt/PKB and PKBR1 in wild-type and *gskA*⁻ cells in response to cAMP. Coomassie Blue staining was used as loading control. (C and D) cAMP-induced Akt/PKB and PKBR1 kinase activity, respectively. H2B was used as substrate; Akt/PKB and PKBR1 protein levels were determined by immunoblotting; for quantification, the maximum value of wild-type cells was taken as 1.0; data are mean ± SE of at least three independent experiments. (E and F) Translocation kinetics of PH_{crac}-GFP (E) and N-termPI3K-GFP (a reporter for PI3K localization) (F) in wild-type and *gskA*⁻ cells in response to cAMP stimulation. The data represent the mean ± SE of relative fluorescence intensity of membrane-localized PH_{crac}-GFP and PI3K-GFP as a function of time after cAMP stimulation with the starting condition taken as 1.0.

DydA function requires GSK-3

Through in vitro and in vivo studies, we verified DydA as a direct target of GSK-3 and show that this phosphorylation is required for many of DydA's functions. As the nonphosphorylatable form of DydA complements some DydA functions and localizes to the cell cortex and appears stable, we do not believe the mutant protein is misfolded. Our data indicate that DydA affects multiple functions required for chemotaxis. On the one hand, it is regulating F-actin polymerization, which seems to be independent of the GSK-3 phosphorylation. On the other hand, DydA is negatively regulating MyoII assembly, a function that is dependent of the phosphorylation by GSK-3.

We observed a small amount of phosphorylation of the GSK-3 site of DydA, even in the absence of GSK-3, and at Ser/Thr residues adjacent to the GSK-3 consensus site. We do not know whether this phosphorylation of DydA in the absence of GSK-3 has any biological relevance, because this phosphorylation appears only in the absence of GSK-3 and our data indicate that under normal conditions, DydA is constitutively phosphorylated, presumably by GSK-3 and a priming kinase. The absence of GSK-3 might make this site accessible to other kinases, resulting in some phosphorylation at sites independent of the GSK-3 consensus site. In addition, there is a GSK-3–like kinase in *Dictyostelium* encoded by the *glkA* gene (DDB_G0270218; Goldberg *et al.*, 2006) that might be responsible for the residual phosphorylation in the absence of GSK-3. We do not know whether GlkA is expressed at aggregation stage or whether it acts as a functional kinase recognizing the same consensus site as GSK-3. The stimulus-independent, constitutive phosphorylation of DydA supports the role of GSK-3 as a permissive signal as proposed by Teo *et al.* (2010). However, we cannot exclude the possibility that DydA phosphorylation is dynamically regulated with a rapid cycle of phosphorylation/dephosphorylation.

GSK-3 is a major regulator of chemotaxis in *Dictyostelium*

Little was understood about the function of GSK-3 in chemotaxis in *Dictyostelium*. Our study uncovered a new component of the GSK-3 regulatory network that helps mediate chemotaxis. Previous studies had demonstrated that *gskA*$^-$ cells have highly aberrant chemotaxis, and one suggested this was due to a loss of PI3K regulation and could be suppressed by overexpression of inositol monophosphatase (IMP-A), which increases PI(3,4,5)P_3 by increasing the levels of the PI3K substrate PI(4,5,)P_2 (Teo *et al.*, 2010). As increased PI(3,4,5)P_3 can cause gain-of-function phenotypes, it is possible that the suppression of the *gskA*$^-$ chemotactic phenotype by IMP-A may be indirect. Others' findings and our own suggest that PI(3,4,5)P_3 levels are reduced two- to threefold based on PH-domain localization studies (Teo *et al.*, 2010). However, as loss of PI3K has only modest effects on chemotaxis in step gradients (Funamoto *et al.*, 2002; Hoeller and Kay, 2007; Takeda *et al.*, 2007; Veltman *et al.*, 2008), it is unlikely that decreased PIP_3 results in the severe *gskA*$^-$ phenotypes.

We provide evidence that Ras activity is highly aberrant in *gskA*$^-$ cells, suggesting a basis for the severe defects in directional sensing observed in the *gskA*$^-$ cells. The high basal Ras activity measured using the RBD_{Byr} might be due to an up-regulation of basal RasC activity. The RasC effector TORC2 was thought to be inactive in the *gskA*$^-$ cells (Teo *et al.*, 2010), but in our hands, TORC2 was activated in the absence of GSK-3 and strongly phosphorylated the HM of Akt/PKB and PKBR1. This is thought to be a prerequisite for the AL phosphorylation mediated by the two PDK1 isoforms, PdkA and PdkB (Kamimura *et al.*, 2008; Liao *et al.*, 2010). PdkA mainly phosphorylates the AL of Akt/PKB and only partially affects PKBR1 phosphorylation, whereas PdkB exclusively phosphorylates the AL of PKBR1. Kimimura and Devreotes (2010) demonstrated that transient PdkA activation is independent of PI(3,4,5)P_3 and TORC2, but that RasC may directly affect PdkA activity (Kamimura and Devreotes, 2010). Therefore increased RasC activity in the *gskA*$^-$ cells might lead to increased PdkA activity and higher phosphorylation of the AL of Akt/PKB and higher Akt/PKB activity. Because the AL of PKBR1 is also phosphorylated by PdkB, effects are less prominent for PKBR1 AL phosphorylation. At this point, we do not know how GSK-3 might affect RasC activity. It was unexpected that the highly increased and extended activity of Akt/PKB and PKBR1 in *gskA*$^-$ cells did not lead to severe changes in F-actin polymerization. It might be possible that the dramatic decrease in PI(3,4,5)P_3 counterbalances the effects of increased Akt/PKB and PKBR1 activity on F-actin polymerization.

Our findings that cells expressing the nonphosphorylatable form of DydA exhibit extended AL and HM phosphorylation suggest that DydA might mediate, in part, GSK-3's role in the regulation of the phosphorylation of PKB and PKBR1. In addition, the effect of GSK-3 on MyoII assembly might be mediated through DydA, since DydA lacking both RA domains exhibits a similar defect in MyoII assembly. It is clear that the phenotype of *gskA*$^-$ cells is complex, and GSK-3 most likely functions through a number of substrates, including DydA, as part of a larger network that controls chemotaxis. Our phosphoproteomic analysis suggests additional substrates for GSK-3. However, additional biochemical and genetic analyses will be required to demonstrate these are bona fide GSK-3 substrates and that phosphorylation by GSK-3 is required for their function.

MATERIALS AND METHODS

Cell culture

Cells were grown in axenic HL5 medium at 22°C. For the expression of GFP- or epitope-tagged proteins, 20 µg/ml Geneticin (Gibco, Grand Island, NY) was added. Knockout cell lines were selected with 7.5 µg/ml blasticidin S. For obtaining aggregation-competent cells, log-phase vegetative cells were washed with 12 mM Na/K phosphate buffer, resuspended at 5×10^6 cells/ml in 12 mM Na/K phosphate buffer, and pulsed with 30 nM cAMP at 6-min intervals for 5.5 h. Aggregation-competent cells were used for the assays unless otherwise indicated.

Strains and constructs

Ax-2 or KAx-3 were used as wild-type. *gskA*$^-$ cells were obtained from the *Dictyostelium* Stock Center. We confirmed that these were *gskA*$^-$ cells by Southern analysis. We also did not identify any GskA peptides identified in wild-type cells in the *gskA*$^-$ strain using mass spectrometry, confirming that the protein was not present at detectable levels (unpublished data). We also tested the *gskA*$^-$ strain for the expression of two aggregation genes (encoding the phosphodiesterase [PDE] psdA and the adenylyl cyclase AcaA) under our conditions used to study *gskA*$^-$ cells (5.5. h cAMP pulsing), which were found previously to be poorly expressed in *gskA*$^-$ cells plated for development compared with wild-type cells (Teo *et al.*, 2010). We found that AcaA exhibited normal expression, while psdA expression was not normal (Figure S2D). We assume the difference between our results and those of Teo *et al.* (2010) are due to different conditions of development between the experiments reported here and those of Teo *et al.* (2010).

Gene disruption for DydA was performed by insertion of a blasticidin-S resistance cassette at base pair 561. Clones were selected in the presence of blasticidin S, and gene disruption was confirmed by PCR and Southern blotting. DydA was cloned from cDNA

(3636 base pairs). Deletion constructs and constructs carrying point mutations for DydA were generated using QuikChange site-directed mutagenesis (Stratagene, Agilent, Santa Clara, CA). For DydA, the following deletions were generated:

DydAΔRA1 + 2: deletion of base pairs 13–270 + 3334–3558 (aa 5–90 + 1112–1196)

DydAΔPH: deletion of base pairs 397–675 (aa 133–225)

DydAΔCH1 + 2: deletion of base pairs 835–1500 (aa 279–500)

DydAΔPRM: deletion of base pairs 1756–2106 (aa 586–702)

GFP- or His-HA-FLAG (HHF) epitope-tagged versions of Daydreamer were generated in Exp-4 (obtained from the *Dictyostelium* Stock Center) carrying 3′ tags for GFP or HHF. GST-DydA$^{1\text{-}798}$ (aa 1–266) and the constructs for the yeast two-hybrid system were generated using Gateway Cloning (Invitrogen, Carlsbad, CA), with pDEST21 as the entry vector and pDEST15 or pDEST22 and pDEST32 as the expression vector(s).

Chemotaxis and cell motility

Chemotactic analysis, the analysis of the global response to a chemoattractant, and vegetative cell motility analysis were performed as previously described (Chung and Firtel, 1999; Sasaki *et al.*, 2007; Wessels *et al.*, 1998; Zhang *et al.*, 2008).

Coimmunoprecipitation

Log-phase vegetative cells (1×10^8) were washed with 12 mM Na/K phosphate buffer and lysed in lysis buffer (50 mM HEPES, pH 8, 150 mM NaCl, 0.5% Triton-X100, 10% glycerol, protease inhibitors, phosphatase inhibitors) for 1 h at 4°C. For coimmunoprecipitation after stimulation, aggregation-competent cells were stimulated with 1 μM cAMP, different time points were collected, and the cells were lysed in lysis buffer for 1 h at 4°C on a rotator. After centrifugation, the supernatant was incubated with 40 μl of 50% FLAG-agarose beads (Sigma-Aldrich, St. Louis, MO) for 1 h at 4°C on a rotator. The beads were washed three times with lysis buffer and used for kinase assays or phosphatase treatment.

Phosphatase treatment

After coimmiunoprecipitation, the beads were washed once in lysis buffer without phosphatase inhibitors and once in phosphatase buffer and then incubated with 800 U λ-protein phosphatase (NEB, Ipswich, MA) for 30 min at 37°C. The beads were resuspended in SDS-sample buffer and separated on SDS–PAGE, and the protein was detected with α-FLAG M2 antibody (Sigma-Aldrich).

In vitro kinase assay

After coimmunoprecipitation, the beads were washed once in kinase buffer (5 mM MOPS, pH 7.2, 2.5 mM β-glycerophosphate, 1 mM ethylene glycol tetraacetic acid (EGTA), 0.4 mM EDTA, 4 mM $MgCl_2$, 0.05 mM dithiothreitol [DTT], 40 ng/μl bovine serum albumin) and then incubated with 100 ng human recombinant GSK-3β (Cell Signaling Technology, Danvers, MA) in the presence of radioactively labeled ATP (250 μM, 2 μCi/ μl) for 20 min at room temperature. All liquid was removed, the beads were resuspended in SDS-sample buffer, and the proteins were separated on SDS–PAGE. The signals were detected by autoradiography.

Ras and Rap1 activity assays

Ras activity assays were performed as previously described (Sasaki *et al.*, 2004; Zhang *et al.*, 2008). Rap1 activity assays were performed as described previously (Jeon *et al.*, 2007). The experiment was repeated at least three times on separate days with internal wild-type controls. The Western blots were quantified using ImageJ.

F-actin polymerization and MyoII assembly

Log-phase vegetative cells were washed with 12 mM Na/K phosphate buffer and resuspended at 5×10^6 cells/ml in 12 mM Na/K phosphate buffer. The cells were starved for 1 h and then pulsed with 30 nM cAMP at 6-min intervals for 4.5 h. The cells were washed once with 12 mM Na/K phosphate buffer and incubated for 30 min before stimulation. After cells were stimulated with 1 μM cAMP, different time points were collected, and cytoskeletal proteins were isolated as described previously (Steimle *et al.*, 2001). The samples were separated on SDS–PAGE and stained with Coomassie Blue. Protein amounts were quantified using ImageJ. The experiment was repeated at least three times on separate days with internal wild-type controls.

Phalloidin staining

Phalloidin staining was performed as described previously (Chung *et al.*, 2000).

Akt/PKB kinase activity assay

Akt/PKB and PKBR1 kinase activities were performed and analyzed as described previously (Meili *et al.*, 1999). H2B was used as a substrate. The experiment was repeated at least 3 times on separate days with internal wild-type controls. The Western blots were quantified using ImageJ.

PKB/PKBR1 phosphorylation

Aggregation-competent cells were stimulated with 1 μM cAMP. Different time points after stimulation were lysed in 2× SDS-sample buffer, and equal amounts of total protein were separated on SDS–PAGE. Phosphorylation of Akt/PKB and PKBR1 at the HM was detected using α-phospho-p70 S6 kinase antibody (Cell Signaling Technology, Danvers, MA), and phosphorylation at the AL was detected using α–phospho-protein kinase C (pan) antibody (Cell Signaling Technology; Kamimura *et al.*, 2008). Coomassie Blue staining of total proteins was used as loading control. The experiment was repeated at least three times on separate days with internal wild-type controls. The Western blots were quantified using ImageJ.

Lipid-binding assay

GST-DydA$^{1\text{-}798}$ and GST alone were expressed in bacteria and purified using glutathione-Sepharose 4B beads (GE Healthcare, Waukesha, WI) according to the manufacturer's protocol. PIP strips from Echelon Biosciences (Salt Lake City, UT) were incubated with 0.5 μg/ml protein following the provided protocol. The GST proteins were detected using α-GST antibody (Cell Signaling Technology).

Pull-down experiments

N-terminal GFP-tagged DydRa1 and DydRA2 were expressed in *Dictyostelium* from the previously published pDM317 plasmid (Veltman *et al.*, 2009). Cells were lysed by incubation in lysis buffer (10 mM Na_2HPO_4, pH 7.2, 1% Triton X-100, 10% glycerol, 150 mM NaCl, 10 mM $MgCl_2$, 1 mM EDTA, 1 mM Na_3VO_4, 5 mM NaF, and protease inhibitor cocktail [Roche, Indianapolis, IN]) for 10 min on ice. Unsoluble proteins were spun down, and precleared lysate was used in pull down with different small G-protein samples. GST fusion of c-truncated small G proteins (RapA, RasC, and RasG) were

purified as described before (Kortholt *et al.*, 2006). Proteins were loaded with nucleotides (GDP or GTPγS) by incubation for 1 h at room temperature with 100× excess of the given nucleotide (50 mM Tris, pH 7.5, 50 mM NaCl, 5 mM $MgCl_2$, 10 mM EDTA, 5 mM DTT), and the reaction was stopped by adding $MgCl_2$ to a final concentration of 20 mM. Proteins were prebound to GSH beads (GE Healthcare) for 1 h at 4°C, and unbound fraction was washed away with PBS. Beads were subsequently mixed with *Dictyostelium* cell lysates and incubated 4°C overnight with rotation. PBS washing steps were performed to wash away the unbound proteins, and beads were boiled in 1× SDS loading buffer. Prey and bait proteins were detected by means of Western blotting with GFP- or GST-specific antibodies (SC9996 [Santa Cruz Biotechnology, Santa Cruz, CA] or 27-4577-01 [GE Healthcare]).

Protein purification and GDI assays

DydRA1 and DydRA2 were expressed from a pGEX4T1 plasmid containing an N-terminal GST and Tobacco Etch Virus (TEV) cleavage side. Proteins were isolated by glutathione affinity purification, proteolytic cleavage, and size exclusion chromatography as previously described (Kortholt *et al.*, 2006). The purified proteins were analyzed by SDS–PAGE, and the concentration was determined by Bradford's method (Bio-Rad, Hercules, CA). The purified protein was used in a GDI assay as previously described (Kortholt *et al.*, 2006).

Mass spectrometry and phosphopeptide analysis

For the phosphoproteomics assay, samples were prepared as previously described (Charest *et al.*, 2010). Phosphopeptide analysis was performed as described previously (Para *et al.*, 2008). Briefly, we lysed aggregation-competent Ax-2 and *gskA*$^-$ cells before and after stimulation with cAMP. After tryptic digestion, the phosphopeptides were enriched, and the samples were analyzed with liquid chromatography–tandem mass spectrometry. The raw data were searched against the sequences from dictyBase (Eichinger *et al.*, 2005) using Spectrum Mill software (Agilent Technologies, Inc. Santa Clara, CA).

ACKNOWLEDGMENTS

We thank Bernd Gilsbach for his assistance with some of the experiments. This work was supported by research grants from the U.S. Public Health Service to R.A.F. and to A.K. V.K. was supported, in part, by a postdoctoral fellowship from the Deutsche Forschungsgemeinschaft.

REFERENCES

Blagg SL, Stewart M, Sambles C, Insall RH (2003). PIR121 regulates pseudopod dynamics and SCAR activity in *Dictyostelium*. Curr Biol 13, 1480–1487.

Bolourani P, Spiegelman GB, Weeks G (2006). Delineation of the roles played by RasG and RasC in cAMP-dependent signal transduction during the early development of *Dictyostelium discoideum*. Mol Biol Cell 17, 4543–4550.

Bolourani P, Spiegelman GB, Weeks G (2008). Rap1 activation in response to cAMP occurs downstream of Ras activation during *Dictyostelium* aggregation. J Biol Chem 283, 10232–10240.

Böttcher RT, Niehrs C (2005). Fibroblast growth factor signaling during early vertebrate development. Endocr Rev 26, 63–77.

Cai H, Das S, Kamimura Y, Long Y, Parent CA, Devreotes PN (2010). Ras-mediated activation of the TORC2-PKB pathway is critical for chemotaxis. J Cell Biol 190, 233–245.

Chang C, Adler CE, Krause M, Clark SG, Gertler FB, Tessier-Lavigne M, Bargmann CI (2006). MIG-10/Lamellipodin and AGE-1/PI3K promote axon guidance and outgrowth in response to Slit and Netrin. Curr Biol 16, 854–862.

Charest PG, Shen Z, Lakoduk A, Sasaki AT, Briggs SP, Firtel RA (2010). A Ras signaling complex controls the RasC-TORC2 pathway and directed cell migration. Dev Cell 18, 737–749.

Chen L, Iijima M, Tang M, Landree MA, Huang YE, Xiong Y, Iglesias PA, Devreotes PN (2007). PLA2 and PI3K/PTEN pathways act in parallel to mediate chemotaxis. Dev Cell 12, 603–614.

Chung CY, Firtel RA (1999). PAKa, a putative PAK family member, is required for cytokinesis and the regulation of the cytoskeleton in *Dictyostelium discoideum* cells during chemotaxis. J Cell Biol 147, 559–576.

Chung CY, Lee S, Briscoe C, Ellsworth C, Firtel RA (2000). Role of Rac in controlling the actin cytoskeleton and chemotaxis in motile cells. Proc Natl Acad Sci USA 97, 5225–5230.

Cross DA, Alessi DR, Cohen P, Andjelkovich M, Hemmings BA (1995). Inhibition of glycogen synthase kinase-3 by insulin mediated by protein kinase B. Nature 378, 785–789.

Eccles SA (2004). Parallels in invasion and angiogenesis provide pivotal points for therapeutic intervention. Int J Dev Biol 48, 583–598.

Eichinger L *et al.* (2005). The genome of the social amoeba *Dictyostelium discoideum*. Nature 435, 43–57.

Embi N, Rylatt DB, Cohen P (1980). Glycogen synthase kinase-3 from rabbit skeletal muscle. Separation from cyclic-AMP-dependent protein kinase and phosphorylase kinase. Eur J Biochem 107, 519–527.

Frame S, Cohen P, Biondi RM (2001). A common phosphate binding site explains the unique substrate specificity of GSK3 and its inactivation by phosphorylation. Mol Cell 7, 1321–1327.

Friedberg F, Rivero F (2009). Single and multiple CH (calponin homology) domain containing multidomain proteins in *Dictyostelium discoideum:* an inventory. Mol Biol Rep 37, 2853–2862.

Funamoto S, Meili R, Lee S, Parry L, Firtel RA (2002). Spatial and temporal regulation of 3-phosphoinositides by PI 3-kinase and PTEN mediates chemotaxis. Cell 109, 611–623.

Ginger RS, Dalton EC, Ryves WJ, Fukuzawa M, Williams JG, Harwood AJ (2000). Glycogen synthase kinase-3 enhances nuclear export of a *Dictyostelium* STAT protein. EMBO J 19, 5483–5491.

Goldberg JM, Manning G, Liu A, Fey P, Pilcher KE, Xu Y, Smith JL (2006). The *Dictyostelium* kinome—analysis of the protein kinases from a simple model organism. PLoS Genet 2, e38.

Grimson MJ, Coates JC, Reynolds JP, Shipman M, Blanton RL, Harwood AJ (2000). Adherens junctions and β-catenin-mediated cell signalling in a non-metazoan organism. Nature 408, 727–731.

Harwood AJ, Plyte SE, Woodgett J, Strutt H, Kay RR (1995). Glycogen synthase kinase 3 regulates cell fate in *Dictyostelium*. Cell 80, 139–148.

Hemmings BA, Yellowlees D, Kernohan JC, Cohen P (1981). Purification of glycogen synthase kinase 3 from rabbit skeletal muscle. Copurification with the activating factor (FA) of the (Mg-ATP) dependent protein phosphatase. Eur J Biochem 119, 443–451.

Hoeller O, Kay RR (2007). Chemotaxis in the absence of PIP3 gradients. Curr Biol 17, 813–817.

Janetopoulos C, Firtel RA (2008). Directional sensing during chemotaxis. FEBS Lett 14, 2075–208.

Jeon TJ, Lee D, Merlot S, Weeks G, Firtel RA (2007). Rap1 controls cell adhesion and cell motility through the regulation of myosin II. J Cell Biol 176, 1021–1033.

Jope RS, Johnson GV (2004). The glamour and gloom of glycogen synthase kinase-3. Trends Biochem Sci 29, 95–102.

Kae H, Lim CJ, Spiegelman GB, Weeks G (2004). Chemoattractant-induced Ras activation during *Dictyostelium* aggregation. EMBO Rep 5, 602–606.

Kamimura Y, Devreotes PN (2010). Phosphoinositide dependent protein kinase (PDK) activity regulates PIP3-dependent and -independent protein kinase B activation and chemotaxis. J Biol Chem 285, 7938–7946.

Kamimura Y, Xiong Y, Iglesias PA, Hoeller O, Bolourani P, Devreotes PN (2008). PIP3-independent activation of TorC2 and PKB at the cell's leading edge mediates chemotaxis. Curr Biol 18, 1034–1043.

Kawata T, Shevchenko A, Fukuzawa M, Jermyn KA, Totty NF, Zhukovskaya NV, Sterling AE, Mann M, Williams JG (1997). SH2 signaling in a lower eukaryote: a STAT protein that regulates stalk cell differentiation in *Dictyostelium*. Cell 89, 909–916.

Kim L, Brzostowski J, Majithia A, Lee N-S, McMains V, Kimmel AR (2011). Combinatorial cell-specific regulation of GSK3 directs cell differentiation and polarity in *Dictyostelium*. Development 138, 421–430.

Kim WY, Wang X, Wu Y, Doble BW, Patel S, Woodgett JR, Snider WD (2009). GSK-3 is a master regulator of neural progenitor homeostasis. Nat Neurosci 12, 1390–1397.

Kölsch V, Charest PG, Firtel RA (2008). The regulation of cell motility and chemotaxis by phospholipid signaling. J Cell Sci 121, 551–559.

Kortholt A, Rehmann H, Kae H, Bosgraaf L, Keizer-Gunnink I, Weeks G, Wittinghofer A, Van Haastert PJ (2006). Characterization of the GbpD-activated Rap1 pathway regulating adhesion and cell polarity in *Dictyostelium discoideum*. J Biol Chem 281, 23367–23376.

Kozlovsky N, Belmaker RH, Agam G (2002). GSK-3 and the neurodevelopmental hypothesis of schizophrenia. Eur Neuropsychopharmacol 12, 13–25.

Krause M *et al*. (2004). Lamellipodin, an Ena/VASP ligand, is implicated in the regulation of lamellipodial dynamics. Dev Cell 7, 571–583.

Lafuente EM, van Puijenbroek AA, Krause M, Carman CV, Freeman GJ, Berezovskaya A, Constantine E, Springer TA, Gertler FB, Boussiotis VA (2004). RIAM, an Ena/VASP and Profilin ligand, interacts with Rap1-GTP and mediates Rap1-induced adhesion. Dev Cell 7, 585–595.

Lee S, Comer FI, Sasaki A, McLeod IX, Duong Y, Okumura K, Yates, 3rd JR, Parent CA, Firtel RA (2005). TOR complex 2 integrates cell movement during chemotaxis and signal relay in *Dictyostelium*. Mol Biol Cell 16, 4572–4583.

Lee S, Parent CA, Insall R, Firtel RA (1999). A novel Ras-interacting protein required for chemotaxis and cyclic adenosine monophosphate signal relay in *Dictyostelium*. Mol Biol Cell 10, 2829–2845.

Liao X-H, Buggey J, Kimmel AR (2010). Chemotactic activation of *Dictyostelium* AGC-family kinases AKT and PKBR1 requires separate but coordinated functions of PDK1 and TORC2. J Cell Sci 123, 983–992.

Lyulcheva E, Taylor E, Michael M, Vehlow A, Tan S, Fletcher A, Krause M, Bennett D (2008). *Drosophila* pico and its mammalian ortholog lamellipodin activate serum response factor and promote cell proliferation. Dev Cell 15, 680–690.

Manoukian AS, Woodgett JR (2002). Role of glycogen synthase kinase-3 in cancer: regulation by Wnts and other signaling pathways. Adv Cancer Res 84, 203–229.

Martin P, Parkhurst SM (2004). Parallels between tissue repair and embryo morphogenesis. Development 131, 3021–3034.

Meili R, Ellsworth C, Firtel RA (2000). A novel Akt/PKB-related kinase is essential for morphogenesis in *Dictyostelium*. Curr Biol 10, 708–717.

Meili R, Ellsworth C, Lee S, Reddy TB, Ma H, Firtel RA (1999). Chemoattractant-mediated transient activation and membrane localization of Akt/PKB is required for efficient chemotaxis to cAMP in *Dictyostelium*. EMBO J 18, 2092–2105.

Pap M, Cooper GM (1998). Role of glycogen synthase kinase-3 in the phosphatidylinositol 3-kinase/Akt cell survival pathway. J Biol Chem 273, 19929–19932.

Papkoff J, Aikawa M (1998). WNT-1 and HGF regulate GSK3 beta activity and beta-catenin signaling in mammary epithelial cells. Biochem Biophys Res Commun 247, 851–858.

Para A, Krischke M, Merlot S, Shen Z, Oberholzer M, Lee S, Briggs S, Firtel RA (2008). *Dictyostelium* Dock180-related RacGEFs regulate the actin cytoskeleton during cell motility. Mol Biol Cell 20, 699–707.

Reymond CD, Gomer RH, Mehdy MC, Firtel RA (1984). Developmental regulation of a *Dictyostelium* gene encoding a protein homologous to mammalian ras protein. Cell 39, 141–148.

Robbins SM, Williams JG, Jermyn KA, Spiegelman GB, Weeks G (1989). Growing and developing *Dictyostelium* cells express different *ras* genes. Proc Natl Acad Sci USA 86, 938–942.

Sarbassov DD, Guertin DA, Ali SM, Sabatini DM (2005). Phosphorylation and regulation of Akt/PKB by the rictor-mTOR complex. Science 307, 1098–1101.

Sasaki AT, Chun C, Takeda K, Firtel RA (2004). Localized Ras signaling at the leading edge regulates PI3K, cell polarity, and directional cell movement. J Cell Biol 167, 505–518.

Sasaki AT, Firtel RA (2006). Regulation of chemotaxis by the orchestrated activation of Ras, PI3K, and TOR. Eur J Cell Biol 85, 873–895.

Sasaki AT, Janetopoulos C, Lee S, Charest PG, Takeda K, Sundheimer LW, Meili R, Devreotes PN, Firtel RA (2007). G protein-independent Ras/PI3K/F-actin circuit regulates basic cell motility. J Cell Biol 178, 185–191.

Steimle PA, Yumura S, Cote GP, Medley QG, Polyakov MV, Leppert B, Egelhoff TT (2001). Recruitment of a myosin heavy chain kinase to actin-rich protrusions in *Dictyostelium*. Curr Biol 11, 708–713.

Takeda K, Sasaki AT, Ha H, Seung H, Firtel RA (2007). Role of phosphatidylinositol 3-kinases in chemotaxis in *Dictyostelium*. J Biol Chem 282, 11874–11884.

Teo R, Lewis KJ, Forde JE, Ryves WJ, Reddy JV, Rogers BJ, Harwood AJ (2010). Glycogen synthase kinase-3 is required for efficient *Dictyostelium* chemotaxis. Mol Biol Cell 21, 2788–2796.

Van Haastert PJM, Keizer-Gunnink I, Kortholt A (2007). Essential role of PI3-kinase and phospholipase A2 in *Dictyostelium discoideum* chemotaxis. J Cell Biol 177, 809–816.

Van Haastert PJM, Veltman DM (2007). Chemotaxis: navigating by multiple signaling pathways. Sci STKE pe40.

Veltman DM, Akar G, Bosgraaf L, Van Haastert PJ (2009). A new set of small, extrachromosomal expression vectors for *Dictyostelium discoideum*. Plasmid 61, 110–118.

Veltman DM, Keizer-Gunnik I, Van Haastert PJM (2008). Four key signaling pathways mediating chemotaxis in *Dictyostelium discoideum*. J Cell Biol 180, 747–753.

Veltman DM, Van Haastert PJM (2006). Guanylyl cyclase protein and cGMP product independently control front and back of chemotaxing *Dictyostelium* cells. Mol Biol Cell 17, 3921–3929.

Wessels D, Voss E, Von Bergen N, Burns R, Stites J, Soll DR (1998). A computer-assisted system for reconstructing and interpreting the dynamic three-dimensional relationships of the outer surface, nucleus and pseudopods of crawling cells. Cell Motil Cytoskel 41, 225–246.

Zhang S, Charest PG, Firtel RA (2008). Spatiotemporal regulation of Ras activity provides directional sensing. Curr Biol 18, 1587–1593.

Zicha D, Dunn G, Brown A (1991). A new direct-viewing chemotaxis chamber. J Cell Sci 99, 769–775.